

See discussions, stats, and author profiles for this publication at: <https://www.researchgate.net/publication/51310840>

# Crystal structure of glutamine phosphoribosylpyrophosphate amidotransferase from Escherichia coli

ARTICLE *in* PROTEIN SCIENCE · JANUARY 1998

Impact Factor: 2.85 · DOI: 10.1002/pro.5560070104 · Source: PubMed

---

CITATIONS

59

---

READS

38

## 5 AUTHORS, INCLUDING:



Juno M Krahm

National Institutes of Health

39 PUBLICATIONS 1,823 CITATIONS

SEE PROFILE

# Crystal structure of glutamine phosphoribosylpyrophosphate amidotransferase from *Escherichia coli*

CHRISTINE R.A. MUCHMORE,<sup>1,3</sup> JOSEPH M. KRAHN,<sup>1</sup> JEONG HYUN KIM,<sup>2,4</sup>  
HOWARD ZALKIN,<sup>2</sup> AND JANET L. SMITH<sup>1</sup>

<sup>1</sup>Department of Biological Sciences, Purdue University, West Lafayette, Indiana 47907

<sup>2</sup>Department of Biochemistry, Purdue University, West Lafayette, Indiana 47907

(RECEIVED May 29, 1997; ACCEPTED July 24, 1997)

## Abstract

Crystal structures of glutamine phosphoribosylpyrophosphate (PRPP) amidotransferase from *Escherichia coli* have been determined to 2.0-Å resolution in the absence of ligands, and to 2.5-Å resolution with the feedback inhibitor AMP bound to the PRPP catalytic site. Glutamine PRPP amidotransferase (GPATase) employs separate catalytic domains to abstract nitrogen from the amide of glutamine and to transfer nitrogen to the acceptor substrate PRPP. The unliganded and AMP-bound structures, which are essentially identical, are interpreted as the inhibited form of the enzyme because the two active sites are disconnected and the PRPP active site is solvent exposed. The structures were compared with a previously reported 3.0-Å structure of the homologous *Bacillus subtilis* enzyme (Smith JL et al., 1994, *Science* 264:1427–1433). The comparison indicates a pattern of conservation of peptide structures involved with catalysis and variability in enzyme regulatory functions. Control of glutaminase activity, communication between the active sites, and regulation by feedback inhibitors are addressed differently by *E. coli* and *B. subtilis* GPATases. The *E. coli* enzyme is a prototype for the metal-free GPATases, whereas the *B. subtilis* enzyme represents the metal-containing enzymes. The structure of the *E. coli* enzyme suggests that a common ancestor of the two enzyme subfamilies may have included an Fe-S cluster.

**Keywords:** allosteric enzyme; complex enzyme; feedback inhibition; Fe-S protein; glutamine amidotransferase; phosphoribosyltransferase; protein crystallography; purine biosynthesis

Glutamine phosphoribosylpyrophosphate amidotransferase catalyzes the first committed step in de novo purine nucleotide synthesis and is the key regulatory enzyme in the pathway. The enzyme catalyzes the transfer of the glutamine amide nitrogen to PRPP to produce phosphoribosylamine, pyrophosphate, and glutamate. GPATase is one of a family of 16 glutamine amidotransferases that utilizes the amide nitrogen of glutamine for biosynthesis of amino acids, nucleotides, amino sugars, and coenzymes (Zalkin, 1993). GPATase sequences have been derived from cloned genes from

more than 20 organisms, including Bacteria, Archea, and Eukarya (Zalkin & Smith, 1998). However, only the enzymes from *Escherichia coli* (Messenger & Zalkin, 1979) and *Bacillus subtilis* (Wong et al., 1981) have been purified to homogeneity and characterized extensively. An X-ray structure has been reported for a nucleotide-inhibited form of the *B. subtilis* GPATase (Smith et al., 1994). The *E. coli* and *B. subtilis* enzymes, which have 39% amino acid sequence identity, are representative of two GPATase classes that are distinguished by an Fe-S cluster and a cleavable NH<sub>2</sub>-terminal propeptide. The *E. coli* GPATase has neither the Fe<sub>4</sub>-S<sub>4</sub> cluster nor the NH<sub>2</sub>-terminal propeptide.

GPATase has two structural domains, an N-terminal glutamine domain that hydrolyzes the amide of glutamine and a C-terminal acceptor domain that utilizes nitrogen released from glutamine or NH<sub>3</sub> from solution for synthesis of PRA. The glutamine domain belongs to an Ntn subfamily of amidotransferases, characterized by an N-terminal catalytic cysteine and eight other invariant residues (Zalkin & Smith, 1998) and belongs also to a more distantly related group of Ntn hydrolases, which utilize an N-terminal nucleophile and have a common three-dimensional structure (Branigan et al., 1995). GPATase is also a phosphoribosyltransferase because it catalyzes phosphoribosyl transfer from PRPP. PRTases

Reprint requests to: Janet L. Smith, Department of Biological Sciences, Purdue University, West Lafayette, Indiana 47907-1392; e-mail: smithj@bragg.bio.purdue.edu.

<sup>3</sup>Present address: Department of Molecular Pharmacology & Biological Chemistry, Northwestern University Medical School, Chicago, Illinois 60611.

<sup>4</sup>Present address: Cellular Oncology R.U., Korea Research Institute of Bioscience and Biotechnology, P.O. Box 115, Yusong, Taejon, 305-600, Korea.

**Abbreviations:** PRPP, phosphoribosylpyrophosphate; GPATase, glutamine PRPP amidotransferase; PRA, phosphoribosylamine; PP<sub>i</sub>, pyrophosphate; PRTase, phosphoribosyltransferase; DON, 6-diazo-5-oxo-L-norleucine; GlmS, glucosamine 6-phosphate synthase; DTT, dithiothreitol; SeMet, selenomethionyl; RMSD, RMS deviation.

are a large enzyme family of nucleotide salvage and synthesis (Musick, 1981). A region of the GPATase acceptor domain and other Type I PRTase enzymes have a common fold. In addition, these enzymes share a conserved fingerprint in the loop to which PRPP binds (Eads et al., 1994; Scapin et al., 1994, 1995; Smith et al., 1994; Henriksen et al., 1996; Schumacher et al., 1996; Somoza et al., 1996; Vos et al., 1997).

We refer to GPATase, as well as the other glutamine amidotransferases, as "complex" enzymes to emphasize that they have separable catalytic domains, each having an active site. The catalytic function of the GPATase glutamine domain is described by a model that is consistent with that for other Ntn amidotransferases (Smith, 1995) and Ntn hydrolases (Brannigan et al., 1995). According to this model, Cys 1 functions as a nucleophile that attacks the carboxamide of glutamine and generates a  $\gamma$ -glutamyl thioester intermediate. Two other conserved residues, Asn 101 and Gly 102, form an oxyanion hole for stabilizing the putative cysteinyl-glutamine tetrahedral intermediate. The side chains of Asp 127 and Arg 73 provide specificity for the  $\alpha$ -amino and  $\alpha$ -carboxyl groups of glutamine. In the glutaminase half reaction, the  $\alpha$ -amino group of Cys 1 serves as the proton donor to the leaving amide group, as proposed for other enzymes in the Ntn hydrolase family (Brannigan et al., 1995).

Catalysis by the PRTases has not been described in such precise structural terms, primarily due to disorder of key residues in the reported structures. These structures share a common theme, in which the well-ordered PRPP site is solvent exposed, but an adjacent loop containing conserved residues is very poorly ordered. This loop has been referred to as the long, flexible loop in the Type I PRTase family (Scapin et al., 1994; Schumacher et al., 1996), and is thought to play a role in shielding PRPP from solvent during catalysis via a substrate-induced ordering. The rapid, nonenzymatic hydrolysis of PRPP in aqueous solution (McClard et al., 1984) has complicated the study of PRTase mechanism and structure.

The key issue in complex enzymes is how the multiple catalytic sites in separate domains are coordinated. For GPATase and other amidotransferases, this question focuses on nitrogen transfer. How does nitrogen transfer take place from glutamine to the acceptor? One possibility is NH<sub>3</sub>-mediated nitrogen transfer, in which the reactions of glutaminase and NH<sub>3</sub>-dependent synthesis of PRA, catalyzed by the two domains, are in some way coupled to give the overall conversion of glutamine and PRPP to PRA, PP<sub>i</sub>, and glutamate. Alternatively, mechanisms for direct nitrogen transfer via nucleophilic attack by the amide of glutamine or activated glutamine on the acceptor have also been considered (Wyngaarden, 1972; Zalkin, 1993; Stoker et al., 1996). In order to distinguish these mechanisms, structural information about the catalytic sites is needed. In the structure of the nucleotide-inhibited *B. subtilis* GPATase (Smith et al., 1994), the glutamine and PRTase active sites are separated by a solvent-accessible space of approximately 15 Å. Are the two catalytic sites in this complex enzyme merged into a single site for direct nitrogen transfer, or is there a mechanism to sequester NH<sub>3</sub> released from glutamine for reaction with PRPP? An X-ray structure is needed for the nucleotide-free, active enzyme. Here we report X-ray structures of the nucleotide-free and AMP-bound *E. coli* enzyme. Concurrent with the structure determinations presented here, the structure of *E. coli* GPATase inactivated by glutamine analogue 6-diazo-5-oxo-L-norleucine was determined in a study of glutaminase function (Kim et al., 1996). Analysis of these structures leads to the conclusion that all are

nonactive conformations. The structures of *E. coli* GPATase reported here should be representative of the enzymes from *Haemophilus*, yeast, and *Neurospora* (Zalkin & Smith, 1998), all of which lack an Fe<sub>4</sub>-S<sub>4</sub> cluster.

## Results and discussion

### Quaternary structure of GPATase

The four subunits of *E. coli* GPATase form a doughnut-shaped tetramer with D<sub>2</sub> molecular symmetry (Fig. 1). The twofold axes are designated P, Q, and R, as for the *B. subtilis* enzyme. PRTase domains interact at the molecular P axis in a "tight" interface, and glutamine domains interact in a "loose" interface at the R axis. The gross similarity of tetrameric aggregation by the *E. coli* and *B. subtilis* enzymes masks substantial differences in subunit interfaces.

The subunit interface at the molecular P axis is directly involved in most GPATase functions. It may contribute to catalysis via the PRTase flexible loop and is involved in feedback inhibition via the allosteric "A" site. The very large buried surface area (2,750 Å<sup>2</sup>/monomer) includes many conserved residues. Nevertheless, the dimer interfaces of PRTase domain cores in the *E. coli* and *B. subtilis* enzymes differ by rotation of 8° and translation of 3.4 Å. In contrast, the subunit interface at the molecular R axis has no clear function. It is formed by nonconserved residues, is distant from active sites and effector binding sites, and buries a rather small surface area (880 Å<sup>2</sup>/monomer). The glutamine domain cores at the molecular R axis differ by rotation of 15° and translation of 10.6 Å between the *E. coli* and *B. subtilis* enzymes. The significant differences in both subunit interfaces were a major obstacle to determination of the initial *E. coli* GPATase crystal structure by molecular replacement.

An apparent discrepancy in the reported aggregation state of *E. coli* GPATase in solution may be resolved by the crystal structures. Messenger and Zalkin (1979) found tetrameric aggregation, and Rudolph and Stubbe (1995) found only dimers. The crystal structures of *E. coli* GPATase include sulfonate-containing buffer molecules in the loose subunit interfaces at the R axis. The Messenger and Zalkin experiments were done in phosphate buffer, which may stabilize the R-axis interface as sulfonate does in crystals, whereas the Rudolph and Stubbe experiments were done in Tris buffer. Sulfonate-containing buffer is not responsible for the observed R-axis interface in crystal structures of *E. coli* GPATase. Isomorphous crystals grown without sulfonate, phosphate, or sulfate have an identical interface (data not shown). The *B. subtilis* enzyme exhibits a concentration-dependent dimer-tetramer equilibrium (Wong et al., 1981). All crystal forms of both enzymes, where the protein concentration approaches 500 mg/mL, are tetrameric. Despite the lack of obvious function for the R-axis interface, the occurrence of similar tetramers in crystals of both the *E. coli* and *B. subtilis* GPATase suggests that this aggregation state may be relevant to the enzyme under some circumstances.

### GPATase subunit structure

The structures of ligand-free and AMP-bound *E. coli* GPATase are nearly identical (Fig. 2A). The subunits of *E. coli* and *B. subtilis* GPATases have similar structures, as expected for proteins with 39% identical sequences. The greatest sequence and structural con-

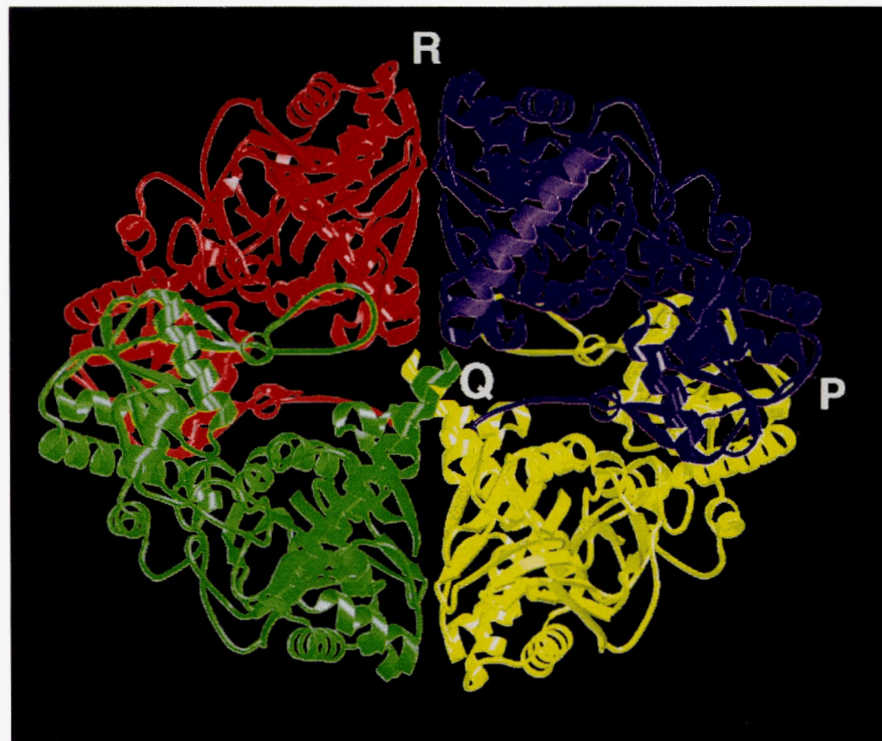


**Fig. 1.** Tetramer of *E. coli* GPATase. The three molecular twofold axes, P, Q, and R, are indicated. Subunits are drawn in contrasting colors.

servation is clustered around the glutamine and PRTase active sites. The 2.0-Å structure of uninhibited *E. coli* GPATase was used as a basis for comparison of structures. Superpositions of the two catalytic domains, based on their structural cores, are shown in Figure 2B and C. The N-terminal glutamine domains have an RMSD of 0.8 Å for a structural core of 158 pairs of  $C_\alpha$  atoms. Excluded from the core are three  $\alpha$ -helices on one side of the domain, which are part of the variable R-axis subunit interface and are positioned differently in the *E. coli* and *B. subtilis* enzymes. The C-terminal PRTase acceptor domains are more similar than the glutamine domains. The RMSD for 101 pairs of  $C_\alpha$  atoms in the PRTase domains is 0.7 Å. Catalytic domain cores of AMP-inhibited and uninhibited *E. coli* GPATase agree within experimental error.

GPATase is expected to exhibit a significant conformational change between the active and inactive states because it is an allosteric enzyme. The hallmark of the inactive conformation of GPATase is a PRTase acceptor active site that is highly exposed to solvent and is distant from the glutamine active site with which its activity must be coupled. Despite the differences in quaternary interactions described above, the overall similarity in conformation of the *E. coli* structures to that of the feedback-inhibited *B. subtilis* enzyme suggests that the structures presented here are also in the inactive conformation. This is supported by the ability of the feedback inhibitor AMP to bind in the P2<sub>1</sub>2<sub>1</sub> crystal form.

AMP is bound to the PRTase domain of only two subunits of the tetramer in the P2<sub>1</sub>2<sub>1</sub> crystal form of *E. coli* GPATase. The subunits with AMP have a hinge between domains that is 2° more open than in the subunits without AMP. The hinges in the two subunits of the uninhibited enzyme (space group C222<sub>1</sub>) are in intermediate positions. AMP-inhibited *B. subtilis* GPATase has an

interdomain hinge that differs from the *E. coli* enzyme structures by 7–8°. Hinging differences between *E. coli* and *B. subtilis* subunits are not with respect to a common axis, and cannot be described as opening or closing.

#### Glutamine domain active site

The glutaminase reaction requires four primary constituents for efficient catalysis: a strong nucleophile, an oxyanion hole to stabilize the presumed tetrahedral intermediate, a proton donor to the NH<sub>3</sub> leaving group, and a binding pocket specific for glutamine. Invariant residues among glutamine amidotransferases of the Ntn family have been proposed to provide these essential elements (Smith, 1995). The structures reported here support this view.

A very unusual feature of the active site of the glutamine domain is its inaccessibility to bulk solvent. This property of the active site is common to all six independent subunits in the two crystal structures reported here, to the two independent subunits of the DON complex (Kim et al., 1996), and to the four independent subunits of the *B. subtilis* GPATase structure (Smith et al., 1994). The glutaminase active site (Fig. 3) lies at one end of a long, narrow cavity in the glutamine domain, near the interface with the C-terminal domain. The cavity is lined with residues that are invariant in the Ntn amidotransferase family: Cys 1, Arg 26, Gly 27, Gly 32, Arg 73, Pro 87, Asn 101, Gly 102, and Asp 127. All atoms of these fingerprint residues superimpose with RMSDs of 0.9–1.0 Å in all GPATase structures. Atomic positions are identical within experimental error (RMSD 0.3 Å) for those residues involved directly in catalysis (Cys 1, Asn 101, and Gly 102). Cys 1, the catalytic nucleophile, is firmly oriented by a hydrogen bond of

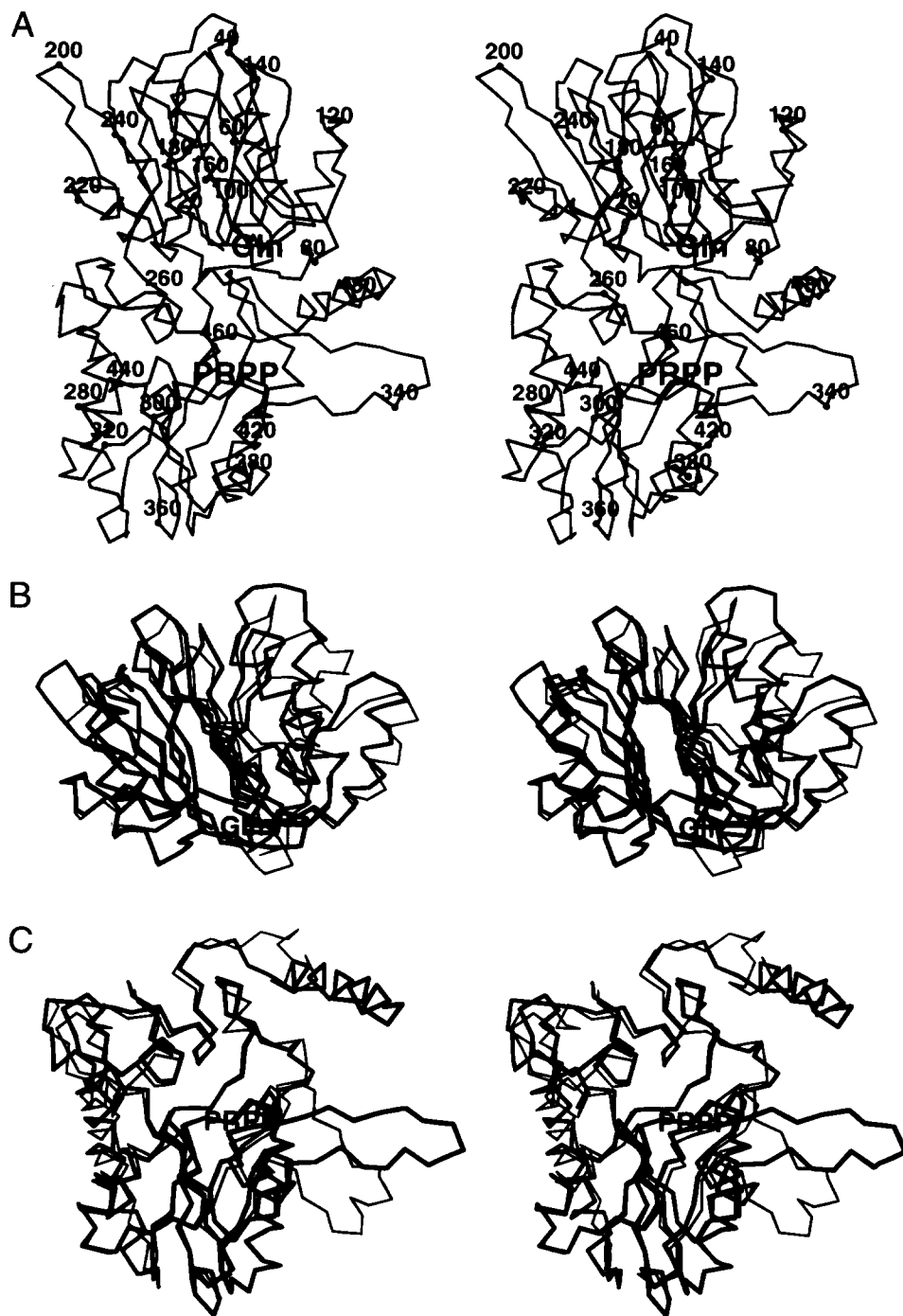


**Fig. 2.** *E. coli* GPATase subunit structure. **A:** Stereo diagram of the  $C_{\alpha}$  trace of the *E. coli* GPATase subunit. Every 20th residue is labeled. Active sites are labeled with the names of their substrates, Gln in the upper glutaminase domain, and PRPP in the lower PRTase domain. **B:** Stereo superposition of the *E. coli* (thick lines) and *B. subtilis* (thin lines) glutamine domains. Superpositions were done for  $C_{\alpha}$  atoms of the structural core, including residues 1–7, 12–36, 40–55, 62–75, 85–91, 95–107, 123–127, 162–172, 177–196, 202–233, and 237–244 of *E. coli* GPATase with residues 1–7, 12–36, 39–54, 61–74, 84–90, 96–108, 123–127, 153–163, 167–186, 187–218, and 221–228, respectively, of *B. subtilis* GPATase. View is rotated approximately 90° about the vertical axis relative to A. The active site is labeled Gln. **C:** Stereo superposition of the *E. coli* (thick lines) and *B. subtilis* (thin lines) PRTase domains. Superpositions were done for  $C_{\alpha}$  atoms of the structural core, including residues 295–324, 355–406, and 421–439 of *E. coli* GPATase with residues 274–303, 334–385, and 400–418, respectively, of *B. subtilis* GPATase. View is similar to that of A. The active site is labeled PRPP.

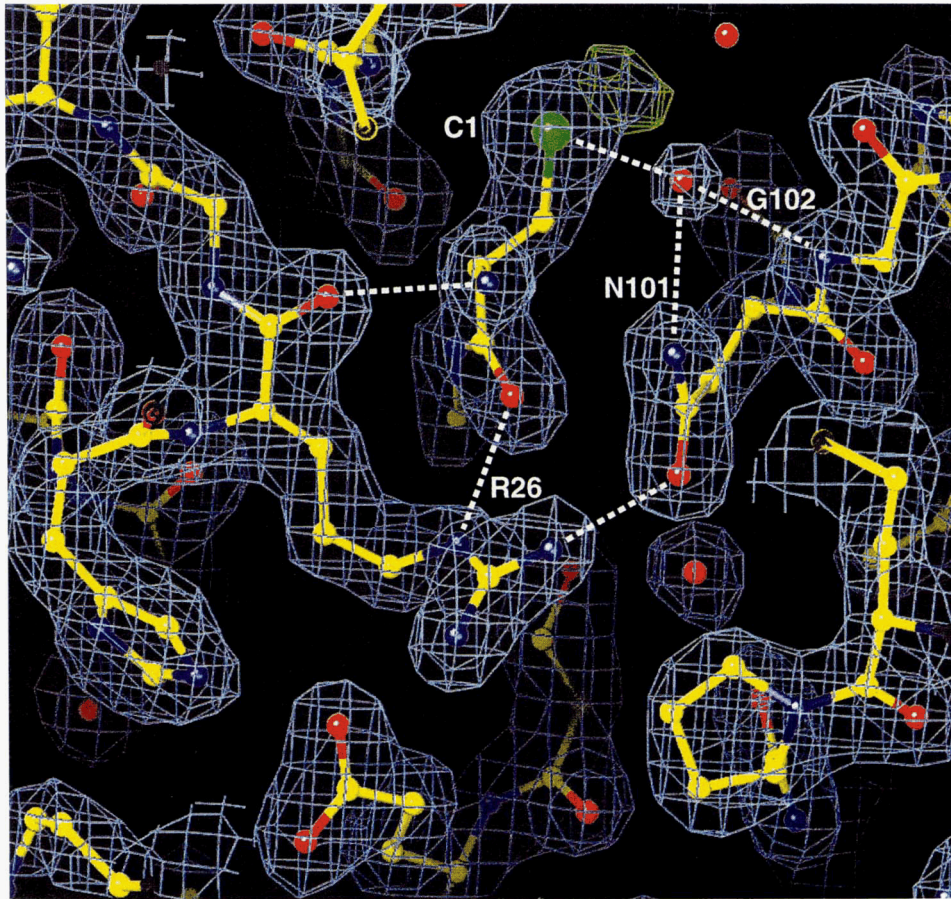


**Fig. 3.** Active site of the glutamine domain of *E. coli* GPATase.  $|2F_{obs} - F_{calc}|$  electron density at 2.0-Å resolution phased with the refined model and contoured in blue at a level of 1.0 RMS is shown for residues around the catalytic Cys 1. Positive  $|F_{obs} - F_{calc}|$  electron density contoured in green at 3.0 RMS illustrates the oxidation of Cys 1  $S_\gamma$ . A water molecule modeled in the oxyanion hole is hydrogen bonded (dashed lines) to  $N_{\delta 2}$  of Asn 101, NH of Gly 102, and  $S_\gamma$  of Cys 1. Arg 26 maintains the structure of the active site via hydrogen bonds to the backbone atoms of Cys 1 and the side chain of Asn 101.

its backbone atoms to Arg 26.  $N_{\delta 2}$  of Asn 101 and the backbone nitrogen of Gly 102 form the oxyanion hole. The orientation of the Asn 101 side chain in the oxyanion hole is fixed by a hydrogen bond to Arg 26. The  $\alpha$ -amino group of Cys 1 is the only group available to function as a proton donor. The side chains of Asp 127 and Arg 73 provide specificity for glutamine via salt bridges, although only the Asp 127 salt bridge occurs in the complex with the glutamine analogue DON (Kim et al., 1996).

GPATase exhibits three levels of glutaminase activity dependent on the state of the acceptor domain. Basal glutaminase is 10- to 20-fold lower than activity stimulated by the acceptor substrate PRPP. The stimulation is due primarily to a decrease in  $K_m$  for glutamine. No glutaminase is detected when nucleotide feedback inhibitors are bound to the acceptor domain. These properties are explained in structural terms by three largely nonconserved peptides lining the active site cavity. The 75–85 flexible loop, the 404–408 loop, and the C-terminal  $\alpha$ -helix have different structures in the *E. coli* and *B. subtilis* enzymes and in different crystal forms of *E. coli* GPATase (data not shown). They form a steric block to the active site, but do not contribute to catalysis or specificity. They also face the acceptor domain and are well positioned to respond to changes in its binding status. For example, Pro 410 is the site of a mutation that blocks nucleotide inhibitor binding

to the active site of the acceptor domain (Zhou et al., 1994). It is likely that transient opening of the flexible, nonconserved peptides accounts for basal glutaminase activity and that nucleotide inhibitor binding fixes the glutaminase active site in a closed state. PRPP binding may stabilize an open conformation of the glutamine site, or a conformation that binds glutamine more effectively.

The crystal structure of the glutamine domain of another Ntn amidotransferase, glucosamine 6-phosphate synthase, was reported recently (Isupov et al., 1996). In this structure of the enzyme-product complex, both elements of glutamine specificity, Arg 73 and Asp 127, form salt bridges with glutamate. Unexpectedly, the catalytic elements of the GlmS active site are positioned differently than in any of the GPATase structures. Cys 1 is rotated away from its presumed catalytic position. The hydrogen bonds from Arg 26 that anchor the backbone atoms of Cys 1 and the side chain of Asn 101 in GPATase are not formed. Isupov et al. (1996) propose that a substrate-induced conformational change brings the catalytic elements of the GlmS active site into positions comparable to those seen in all GPATase structures. However, the active site conformation in the GlmS structure may also be a result of scission of the glutamine domain from the acceptor domain.

Residual electron density near Cys 1 in the uninhibited enzyme structure indicates that  $S_\gamma$  has been oxidized (Fig. 3). A model with

a single oxygen atom at this position (1.5 Å from S<sub>y</sub>) fits the density well and corresponds to sulfenic acid, which is very unstable and would be expected to undergo rapid oxidation to the doubly oxidized sulfinic acid (Kyte, 1995). In this state, the second oxygen would occupy the oxyanion hole. This is consistent with the rather short hydrogen bond between S<sub>y</sub> and the water in the oxyanion hole (2.9 Å). Although sulfinic acids also are oxidized readily to sulfonates, limited solvent access to the enclosed active site and the electronegativity of the oxyanion hole may stabilize the sulfinic acid. Attempts to model various cysteine oxidation states at this site, either singly or as a mixture, were of limited success, and multiple states may be present. The unusual oxidative properties of Cys 1 indicate that the active site environment promotes the nucleophilicity of S<sub>y</sub>. Oxidation of Cys 1 in crystals is consistent with enzyme inactivation by thiols and oxygen (Messenger & Zalkin, 1979). Dithiothreitol was included in the preparation of the SeMet enzyme to protect selenomethionyl residues from oxidation. Residual electron density in this structure suggests a different mixture of states from the wild-type enzyme and is consistent with partial occupancy by a thiol-linked DTT molecule.

#### PRTase active site

The PRTases are enzymes that catalyze pyrophosphoryl transfer from PRPP. Type I PRTases have a common fingerprint for their PRPP binding sites and a common structure. The core structure is a five-stranded, parallel  $\beta$ -sheet. The fingerprint includes the hydrophobic central  $\beta$ -strand, a six-residue loop, and the beginning of an  $\alpha$ -helix. The last residue of the  $\beta$ -strand and first residue of the loop are a pair of acidic side chains in most PRTases, residues Asp 366 and Asp 367 in GPATase. The loop and first turn of  $\alpha$ -helix form the binding site for the ribose 5-phosphate moiety of PRPP, of PRTase products, and of inhibitors (Eads et al., 1994; Scapin et al., 1994, 1995; Smith et al., 1994; Schumacher et al., 1996; Somoza et al., 1996; Chen et al., 1997). This site is occupied by the ribose 5'-phosphate of feedback inhibitor AMP in two subunits of the P2<sub>1</sub>2<sub>1</sub>2<sub>1</sub> crystal form of GPATase (Fig. 4).

An unusual structural feature in a loop adjacent to the PRPP binding site of some PRTases also occurs in GPATase. There is a

*cis* peptide bond between Pro 302 and Glu 303 in all subunits of both crystal forms of *E. coli* GPATase (Fig. 4). The *cis* conformation is highly unusual in any peptide except those preceding a proline residue. An analogous *cis* peptide has been reported in other PRTases (Henriksen et al., 1996; Somoza et al., 1996; Vos et al., 1997) and in *B. subtilis* GPATase (Chen et al., 1997). The independent observation of this highly unusual structural feature in the same topological location of several PRTases is consistent with an important role for the *cis* peptide. The *cis* peptide is positioned to be involved in pyrophosphate binding in the PRPP complexes of PRTases in which it occurs.

GPATase and other Type I PRTases have a long flexible loop between the second and third  $\beta$ -strands of the core  $\beta$ -sheet (Eads et al., 1994; Scapin et al., 1994; Smith et al., 1994; Henriksen et al., 1996; Schumacher et al., 1996; Somoza et al., 1996; Vos et al., 1997). This "PRTase flexible loop" is thought to become ordered during catalysis and to be involved in sequestering the PRTase active site from solvent. However, in none of the reported structures is the flexible loop in a closed conformation. The PRTase flexible loop in GPATase is anchored at its ends in a two-stranded, antiparallel  $\beta$ -sheet between residues 323–327 and 349–353. The 328–348 peptide is very flexible and includes six invariant residues, none with an obvious function in the open, inactive form of the enzyme. Thus, it is not possible to propose a structure-based mechanism for catalysis by the PRTase domain with catalytic roles for specific residues as we have done for the glutamine domain of GPATase. The six invariant residues are presumed to be part of the active site in the closed form of the enzyme.

An unexpected difference between the *E. coli* and *B. subtilis* enzymes is the very different conformations for their PRTase flexible loops, despite sequence identity for 20 of 31 residues (Fig. 5). In all subunits of the *B. subtilis* structure, the loop has a well-ordered conformation resembling a flag. In the structures of the *E. coli* enzyme presented here, much of the flexible loop is poorly ordered. The loop includes most of the surface area buried in the subunit interface at the molecular P axis through interactions with the glutamine domain of the adjacent monomer (Fig. 1). Conserved residues of the flexible loop interact with nonconserved residues of the neighboring monomer. Clearly, the multiple structures of the loop in the inactive forms of GPATase are not relevant

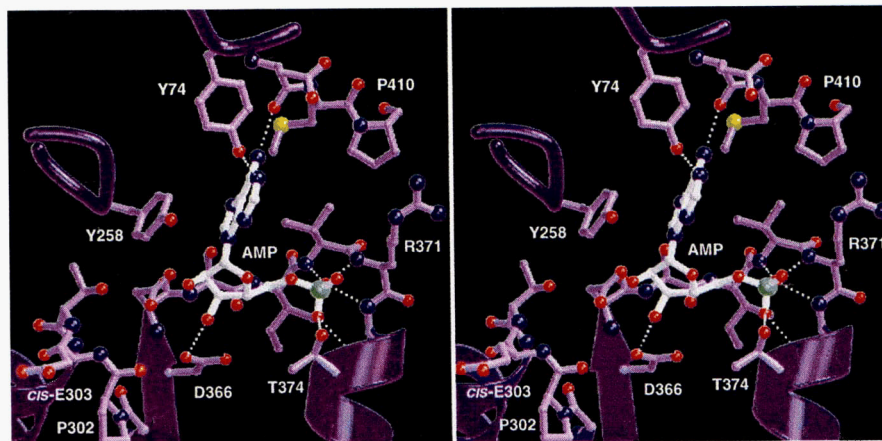


**Fig. 4.** Stereo diagram of AMP binding to the PRPP binding loop of the PRTase domain of GPATase. The *cis* peptide between residues Pro 302 and Glu 303 is visible at the left. Hydrogen bonds are shown as dashed lines.

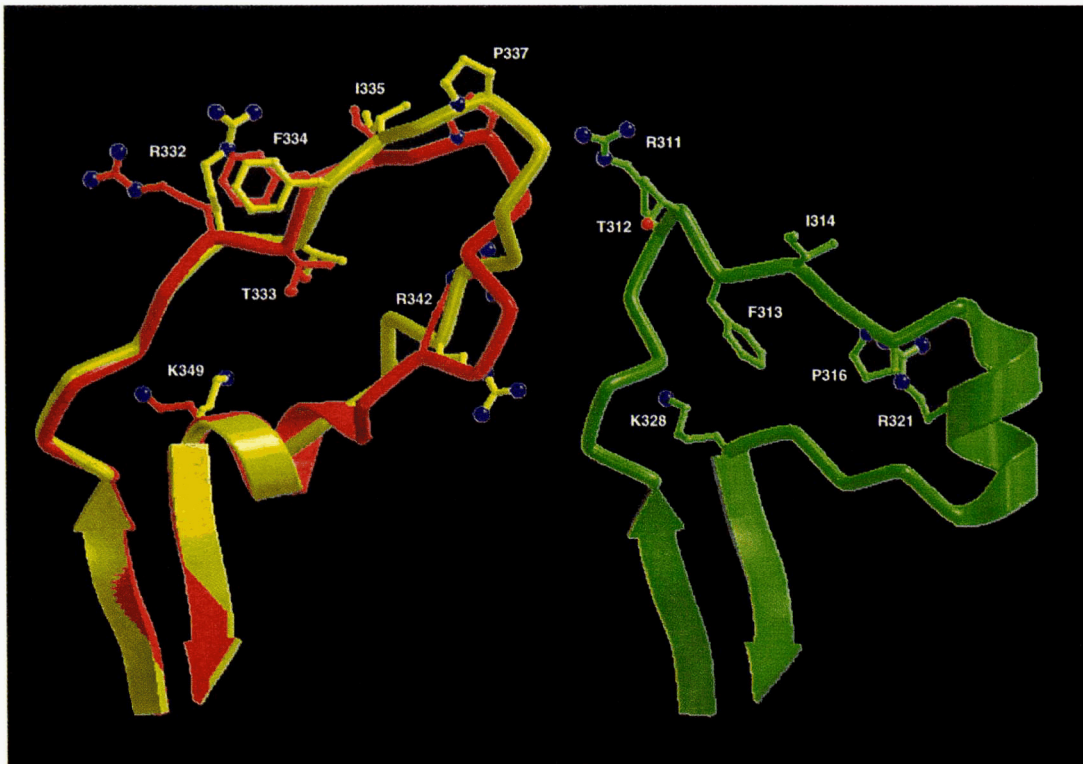


**Fig. 5.** Comparison of conformations of the PRTase flexible loop in *E. coli* and *B. subtilis* GPATases. The *E. coli* flexible loop is shown on the left in yellow for the unliganded enzyme and in red for the AMP-bound enzyme. The *B. subtilis* flexible loop is shown on the right. Side chains of invariant residues are shown explicitly and labeled.

to conservation of its sequence. We anticipate that the structures of the flexible loops are very similar for *E. coli* and *B. subtilis* GPATases in their active forms, with invariant residues of the flexible loop residing in the PRTase active site.

#### Feedback inhibitor binding sites

Feedback regulation of GPATase by purine nucleotide inhibitors occurs at the PRTase acceptor domain. Two different feedback inhibitor binding sites were identified in the structure of the *B. subtilis* enzyme (Smith et al., 1994). These are the catalytic C site, coincident with the PRPP binding site, and the allosteric A site, at the subunit interface of the molecular P axis. These sites are a departure from the usual situation for allosteric proteins, in which effector molecules bind at sites that are remote from the active center and between subunits. Although the A site is between subunits, it is also adjacent to the active site, and the C site directly overlaps the active site. Nucleotide specificity at these sites differs in the *E. coli* and *B. subtilis* enzymes. AMP binds preferentially to the C site and GMP to the A site of *E. coli* GPATase (Zhou et al., 1994), whereas GMP is preferred in the *B. subtilis* C site and ADP in the A site (Chen et al., 1997).

In accord with nucleotide specificity, no nucleotide is bound to the A sites in AMP co-crystals of GPATase (P2<sub>1</sub>2<sub>1</sub> crystal form). AMP is bound in the C sites of two subunits of the tetramer (Fig. 4). There was no electron density corresponding to nucleotide binding in the C sites of the other two subunits, consistent with the 2° dif-

ference in hinge angle between domains of empty and AMP-bound subunits. Interestingly, the tight dimer interface at the molecular P axis includes one subunit with AMP and one without AMP (Fig. 6). In the structure of the uninhibited enzyme (C222<sub>1</sub> crystal form), the sulfonate group of a PIPES buffer molecule is bound in each C site similarly to the AMP phosphate. Although divalent metal ion is required for PRTase catalysis, none is present in either of the enzyme models presented here. Divalent metal ion is incompatible with the P2<sub>1</sub>2<sub>1</sub> crystal form of AMP-inhibited GPATase. No metal sites were apparent in the structure of the uninhibited enzyme, although Mg<sup>2+</sup> was included in crystallization solutions.

AMP binds to the PRPP binding loop via its ribose 5'-phosphate group (Fig. 4). The backbone nitrogens of residues 370, 371, 372, and 374 in the PRPP loop form hydrogen bonds with the AMP phosphate. The dipole of helix 373–387 is oriented to provide additional electrostatic binding energy. A continuum of orientations for nucleotide binding to the PRPP loop of PRTases has been reported (Eads et al., 1994; Scapin et al., 1994; Smith et al., 1994; Schumacher et al., 1996; Somoza et al., 1996; Chen et al., 1997). The orientations differ by rotation of the nucleotide about its 5'-phosphate in the first turn of the  $\alpha$ -helix, much like rotation of a ball-and-socket joint. The structures with the joint rotated so that ribose is closest to the PRPP loop also include Mg<sup>2+</sup> (Tomchick et al., 1994; Schumacher et al., 1996; Chen et al., 1997). In these structures, Mg<sup>2+</sup> is coordinated by the ribose 2'-OH and 3'-OH and by the two acidic side chains that are a hallmark of PRPP loop sequences (Asp 366–Asp 367 of *E. coli* GPATase). Lack of divalent cations in AMP co-crystals of GPATase accounts for the po-

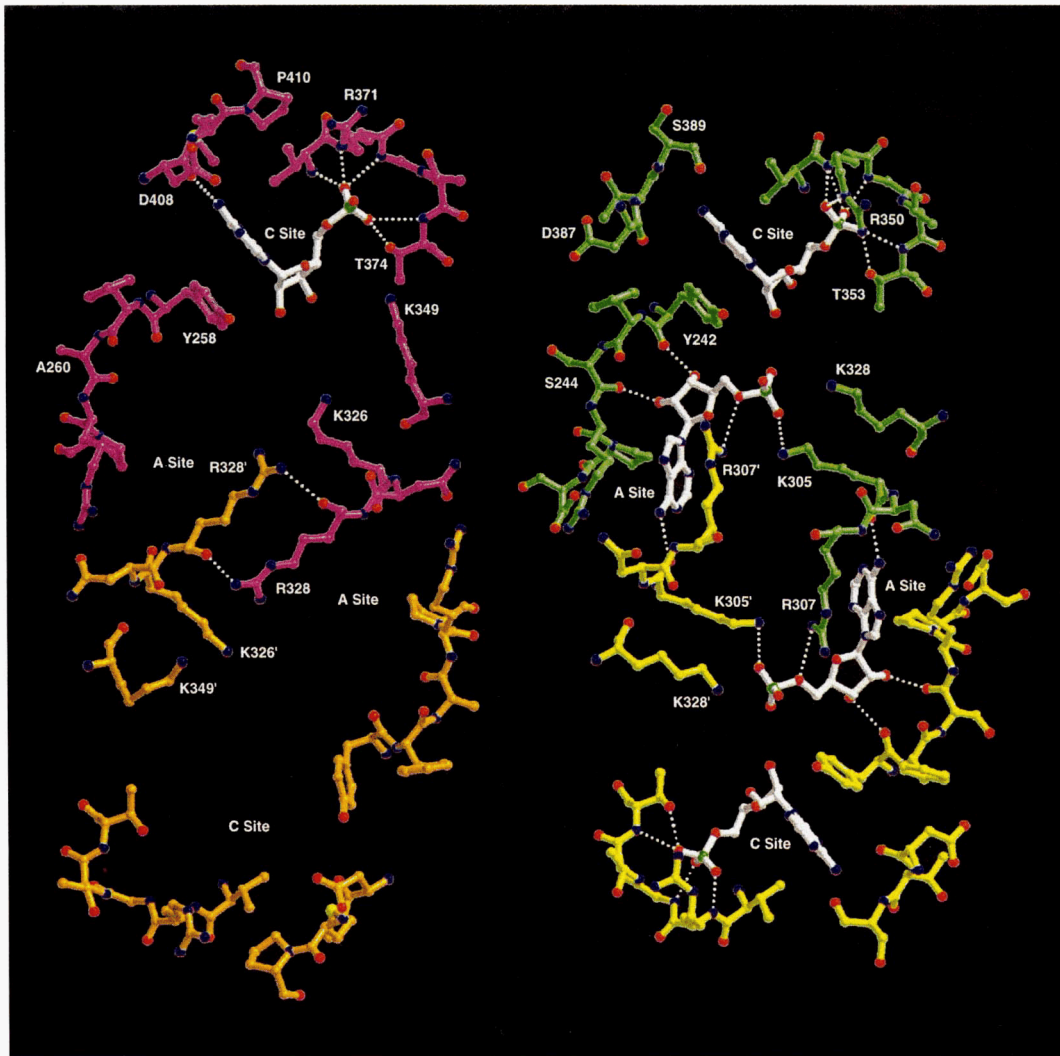


**Fig. 6.** Comparison of nucleotide binding sites in *E. coli* (left) and *B. subtilis* (right) GPATases. View is along the molecular P axis. The proximity of the C and A sites is clear from this diagram, as is the participation of the base-binding peptide in two A sites. Residues discussed in the text are labeled. The AMP molecules are drawn in white bonds, and peptides from different subunits in contrasting colors.

sition of AMP in the PRPP site and for the partial occupancy of the site, estimated to be 40%.

Nucleotide specificity of the A sites can be explained by structural differences between *E. coli* and *B. subtilis* GPATases. A major contributor to the A site is the “anchor” of the PRTase flexible loop, which fixes the ends of the loop in two antiparallel  $\beta$ -strands. The flexible loop of GPATase is adapted for binding feedback inhibitors through its anchor in addition to the presumed substrate binding role of its invariant residues. In *B. subtilis* GPATase, base specificity in the A site is provided by a hydrogen bond to the backbone of residues 305–307 of the anchor, whereas the ribose of the A-site nucleotide binds to residues 242–244 (Fig. 6). The analogous residues of *E. coli* GPATase, 326–328 and 258–260, are positioned to form similar interactions. Use of backbone hydrogen bonding is notable given the differing nucleotide specificity of the *E. coli* and *B. subtilis* A sites. However, the base-binding tripeptide contributes to two A sites and to the subunit interface, and its  $C_\alpha$  atoms are shifted 1.1 Å in *E. coli* GPATase with respect to their counterparts in the

*B. subtilis* enzyme. The substantially different positions for the base-binding peptide relative to the ribose-binding peptide in *E. coli* and *B. subtilis* GPATases may account for observed differences in nucleotide specificities of the A sites. Although the 326–328 tripeptide in the flexible loop anchor has the same sequence (Lys-Asn-Arg) in *E. coli* and *B. subtilis* GPATases, it is not an invariant peptide. Other residues in the subunit interface between PRTase domains are likewise variable. We conclude that variability in this interface is responsible for somewhat different modes of feedback inhibition in GPATase from different sources, which has been examined in detail for only the *E. coli* (Zhou et al., 1994) and *B. subtilis* enzymes (Chen et al., 1997).

#### *Fe<sub>4</sub>-S<sub>4</sub>* cluster

*E. coli* and *B. subtilis* GPATases are prototypes of GPATase subfamilies that, respectively, lack or include a Fe<sub>4</sub>-S<sub>4</sub> cluster. In the *B. subtilis* enzyme, the cluster is near the interdomain connection,

although all four cysteine ligands are from the C-terminal PRTase domain. Conservation of sequence and structure in the PRTase and glutaminase active sites of the *E. coli* and *B. subtilis* enzymes is consistent with the proposal that the Fe<sub>4</sub>-S<sub>4</sub> cluster is not involved in catalysis (Switzer, 1989). Remarkably, the peptides surrounding the cluster in *B. subtilis* GPATase are identical in structure to their counterparts in the *E. coli* enzyme (Fig. 7). This suggests a role for the site in maintaining the structural integrity of the protein. The site in *E. coli* GPATase is filled by three well-ordered water molecules and by the side chains of Arg 188, Cys 252, Asn 403, and Glu 457. The water-filled cavity and similarity in neighboring peptides suggest that a common ancestor of the metal-free and metallo GPATase subfamilies contained an Fe-S cluster in this site. The Fe<sub>4</sub>-S<sub>4</sub> cluster of *B. subtilis* GPATase is thought to be an oxygen sensor that marks the enzyme for degradation (Switzer, 1989). GPATase turnover is regulated differently in *E. coli*, where the enzyme is quite stable in vivo (Messenger & Zalkin, 1979).

#### C-terminal helix

The greatest sequence variability among GPATases occurs at their C-termini, which vary in length from 26 to 69 residues beyond the last element of secondary structure in the PRTase domain core. As a group, the 23 reported GPATase sequences cannot be aligned credibly in this region except for a short, 12-residue peptide, *E. coli* residues 456–467. Like the sequences, the structures of residues 448–505 in *E. coli* and 427–465 in *B. subtilis* GPATase are highly divergent except for the 12-residue peptide, which has both sequence and structural similarity. This peptide includes two of the four cysteine ligands in *B. subtilis* GPATase (Fig. 7). The most variable parts of the C-terminal structures are not part of the PRTase domain, but pack against the N-terminal glutamine domain.

The C-terminal structural element of *E. coli* GPATase is a long  $\alpha$ -helix, beginning at residue 472, continuing away from the body of the subunit, and gradually becoming disordered after residue 492. This unusual helix intersects the molecular Q axis and the C-terminal helix of another subunit near residue Met 500 (Fig. 1). Indeed, continuation of both helices is a steric impossibility and only one of the two Met 500 side chains was visible in SeMet isomorphous difference maps. In all six crystal forms of *E. coli* GPATase, each subunit ends in an  $\alpha$ -helix that is disordered at its C-terminus (data not shown). We infer that the helix is flexible in solution because it packs against the subunit differently in different crystal structures.

Residues 474–482 of the variable C-terminus contact another GPATase peptide, residues 407–414, with divergent structures in the *E. coli* and *B. subtilis* enzymes. In this case, however, the eight loop residues 407–414 have similar sequences in all GPATases. The peptide is bracketed by invariant residues, Gly 406 and Leu 415, which have similar conformations and contacts in the two enzymes. However, the conserved residues Ile 407 and Asp 408 are not structurally equivalent to their apparent counterparts in the *B. subtilis* enzyme, Ile 386 and Asp 387. If the sequence similarity of these peptides has a function, it is not relevant to the inactive forms of the *E. coli* and *B. subtilis* enzymes. The first two residues of the peptide also contribute to the active site cavity in the glutamine domain. Upon enzyme activation, the 407–414 peptide may adopt a conformation different than the inactive form of either *E. coli* or *B. subtilis* GPATase. This peptide also includes Pro 410, which was the site of a mutation designed to eliminate nucleotide binding, but not substrate binding, to the PRTase active site (Zhou et al., 1994).

The C-terminal helix may be part of a signal transduction pathway between the glutaminase and PRTase domains of GPATase.

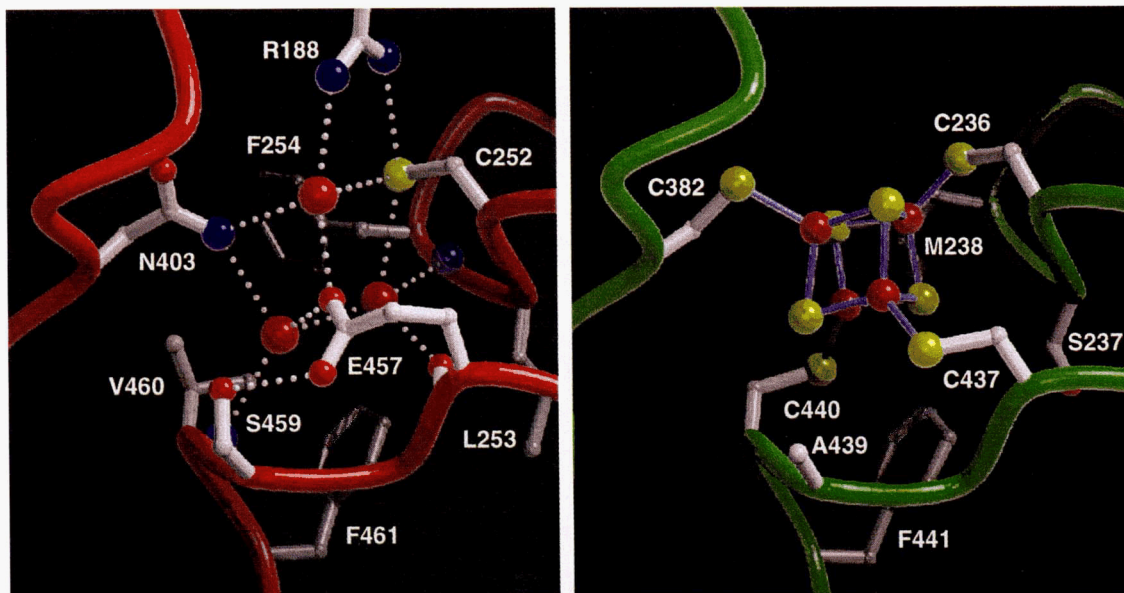


**Fig. 7.** Similarity of peptides at the site of Fe<sub>4</sub>-S<sub>4</sub> cluster binding in *B. subtilis* GPATase (right) and water binding in metal-free *E. coli* GPATase (left). C<sub>α</sub> atoms of 18 residues surrounding the cluster site (251–256, 402–406, and 456–462 of the *E. coli* enzyme with 235–240, 381–385, and 436–442, respectively, of the *B. subtilis* enzyme) superimpose with an RMSD of 0.55 Å. Water molecules are depicted as large red spheres and hydrogen bonds as dotted lines. Coordination bonds of the Fe<sub>4</sub>-S<sub>4</sub> cluster are drawn in solid purple lines.

The helix contacts two peptides of variable sequence and/or structure: the 75–85 flexible loop and the 404–420 peptide. Together with these peptides, the C-terminal helix contributes to closure of the glutaminase active site. These flexible structures may also contribute to PRPP- and inhibitor-modulated access to the glutamine active site by communicating the binding status of the PRTase domain to the glutaminase domain.

### Conclusion

The structures presented here are for an inhibited form of GPATase. In contrast to these structures, the active enzyme must sequester the PRTase reaction from water and form a functional connection between the glutaminase and PRTase active sites. Thus, enzyme activation involves structural changes that are expected to include closure of the PRTase active site in association with ordering the PRTase flexible loop, and opening of a connection between the two active sites.

Comparison of *E. coli* and *B. subtilis* GPATases reveals a pattern of conserved peptides having roles in catalysis and variable peptides that function in regulation. Roles of conserved peptides involved in catalysis are particularly well understood in the glutaminase domain. In the PRTase domain, the PRPP-binding loop has an invariant sequence and structure, but the PRTase flexible loop and 407–415 peptide differ in structure despite their conserved sequences and locations near the active sites. The purpose of their conservation is expected to be relevant to the active form of the enzyme, not to the inactive forms thus far described. Peptides involved in the regulatory functions of the enzyme, on the other hand, are more variable. The flexible 75–85 loop and C-terminal helix control access to the glutamine site and may participate in signaling catalytic readiness of the PRTase domain to the glutaminase domain. They have different sequences and structures in the *E. coli* and *B. subtilis* enzymes. Similarly, the anchor of the PRTase flexible loop has a nonconserved sequence, and contributes to different properties of feedback regulation in different GPATases. The Fe<sub>4</sub>-S<sub>4</sub> cluster may regulate turnover of metallo-GPATases, a function that must be handled otherwise in metal-free GPATases. Thus, the GPATases, represented by the *E. coli* and *B. subtilis* enzymes, have evolved different structural mechanisms for their regulatory functions while conserving the mechanisms of their catalytic functions.

### Materials and methods

#### Protein purification and crystallization

Purified wild-type *E. coli* GPATase was prepared as described (Zhou et al., 1993). SeMet protein was produced by expression of *purF* in the *E. coli* *metA* auxotrophic strain DL41 (Hendrickson et al., 1990) using plasmid pTrcF. In this plasmid, *E. coli* *purF* is under the control of the *trc* promoter in plasmid pTrc99A (Amann et al., 1988). Cells were grown as described (Hendrickson et al., 1990) to mid-log phase (Klett 70). The *purF* gene was induced with 1 mM IPTG and growth was continued for 5–8 h to Klett 85. Protein was purified as for the wild-type enzyme, with the addition of 5 mM DTT to all buffers to prevent oxidation of methionine. DL-selenomethionine was purchased from CalBiochem, and stored at –20 °C as a 10 mg/mL stock solution following filtration through a 0.22-μm filter.

Crystals of the AMP complex (space group P2<sub>1</sub>2<sub>1</sub>2<sub>1</sub>) were grown by sitting drop vapor diffusion, with a reservoir solution of 100 mM MES, 50 mM Tris, 2 mM AMP, 4 mM EDTA, and 15–18% (w/v) PEG 3350 at pH 6.3. Each drop contained 5 μL of reservoir solution and 5 μL of 7–35 mg/mL protein solution. These were incubated at 27 °C for 24 h and then at 21 °C for 7–10 days. Crystals grew up to 0.7 mm in the longest dimension, with all dimensions at least 0.2 mm.

Crystals of unliganded wild-type and selenomethionyl enzyme (space group C222<sub>1</sub>) were grown by vapor diffusion in sitting drops containing 4 μL of 20 mg/mL protein and 4 μL reservoir solution (15% w/v PEG 3350, 5% 2-propanol, 100 mM PIPES, 4 mM MgCl<sub>2</sub>, pH 6.5). Crystals grew in 1–2 weeks at 20 °C.

#### Data collection

The diffraction data set for the P2<sub>1</sub>2<sub>1</sub>2<sub>1</sub> crystal form is a hybrid of high-resolution data collected at the Photon Factory in Tsukuba, Japan, and of low-resolution data collected with multiwire detectors at Purdue University. The multiwire data were measured with a double-detector system (SDMS, AFC6), using CuKα radiation from a Rigaku rotating anode source, and crystal-to-detector distances of 1,005 mm and 945 mm. Crystals were maintained at 14.5 °C (AIR-JET, FTS Systems, Stone Ridge, New York). Weak reflections in these data ( $h + k = \text{odd}$ ) were missed in the indexing, and were integrated and scaled in space group C222<sub>1</sub> using the program XDS (Kabsch, 1988) adapted for the SDMS multiwire detector (D. Diggs & K. Watkins, pers. comm.). Statistics for these data reflect  $h + k = \text{even}$  reflections only. High-resolution data were collected in the Weissenberg geometry on image plates at Photon Factory beamline 6A2 (Sakabe, 1991) with a cylinder radius of 429.7 mm. Image plates (Fuji-Photo Film Co. Ltd.) were scanned with a FUJIX BA100 scanner. Ninety images were integrated as P2<sub>1</sub>2<sub>1</sub>2<sub>1</sub> with the program WEISS (Higashi, 1989), scaled, and reduced with ROTAVATA and AGROVATA from the CCP4 suite (CCP4, 1994). A hybrid data set was created to supplement poorly measured low-resolution data obtained in the Weissenberg geometry. Synchrotron data from 10.0 to 2.5 Å were combined with CuKα data for  $h + k = \text{even}$  reflections from 40.0 to 4.0 Å. Unit cell dimensions of  $a = 118.5$  Å,  $b = 158.2$  Å, and  $c = 107.9$  Å for the P2<sub>1</sub>2<sub>1</sub>2<sub>1</sub> crystal form were determined from refined parameters for 90 synchrotron images because no postrefinement of global parameters was available in the processing program WEISS. Cell constants were adjusted later based on the C222<sub>1</sub> structure. Statistics for individual and merged data are given in Table 1. The crystallographic asymmetric unit includes four 56-kDa subunits with a solvent content of approximately 42%.

C222<sub>1</sub> diffraction data were collected on crystals flash frozen to 110 K with an Oxford Cryostream, using a Rigaku rotating anode CuKα source and an R-AXIS IIc image plate system. Crystals of approximately 0.5 × 0.3 × 0.2 mm were cryoprotected in a solution of 7.5% PEG 3350, 10% 2-propanol, 85 mM PIPES, 14% D,L-meso-2,3-butanediol, and 3.4 mM MgCl<sub>2</sub>. Larger crystals responded poorly in the solution transfers. Complete data sets were obtained from single crystals, with no measurable decay of diffracted intensities during the experiment. Images were integrated and scaled with the HKL data processing package (Otwinowski, 1993; Otwinowski & Minor, 1997). Due to similarity with the P2<sub>1</sub>2<sub>1</sub>2<sub>1</sub> crystal form, images were initially indexed and integrated on a primitive lattice and the integrated intensities were examined to ensure that the C-centering was exact. Statistics for native and

**Table 1.** Summary of diffraction data

	AMP P2 <sub>1</sub> 2 <sub>1</sub>	SeMet	No ligand C222 <sub>1</sub>	Native 1	Native 2
<i>a</i> (Å)	116.8	116.6	116.4	116.9	116.9
<i>b</i> (Å)	156.0	157.3	157.4	157.5	157.5
<i>c</i> (Å)	106.9	106.6	106.5	106.3	106.3
Temperature (°C)	6	-163	-163	-163	-163
No. crystals	10	1	1	1	1
<i>d</i> <sub>min</sub> (Å)	2.5	2.3	2.3	2.0	2.0
<i>R</i> <sub>sym</sub> <sup>a</sup> (%)	6.5	4.5	4.7	4.1	4.1
No. observations	199,847	138,475	164,648	268,969	268,969
No. unique reflections	55,291	38,125	40,345	65,480	65,480
Completeness (%)	77.8	86.8	91.9	98.2	98.2
Average <i>I</i> / <i>σI</i>	37.0	25.5	26.1	20.2	20.2

<sup>a</sup> $R_{sym} = \sum_{hj} |I_h - I_j| / \sum_j I_j$ , where  $I_h$  = average intensity over symmetry-related observations of a reflection with unique indices and  $I_j$  = *j*th observation of a reflection with average intensity  $I_h$ .

selenomethionyl data are given in Table 1. The crystals contain one-half GPATase tetramer per asymmetric unit.

#### Structure determination of the P2<sub>1</sub>2<sub>1</sub> crystal form

The structure of *E. coli* GPATase was solved initially for the P2<sub>1</sub>2<sub>1</sub> crystal form. A self-rotation search for twofold operators was calculated with GLRF (Tong & Rossmann, 1990). Two peaks, at  $\phi = 43^\circ$  and  $47^\circ$ ,  $\psi = 90.0^\circ$  (polar angle convention of Rossmann & Blow, 1962) persisted over various resolution ranges and integration radii. These peaks are consistent with the expected molecular 222 symmetry with one axis parallel to the crystallographic *b* axis. A probe model was constructed from the crystal structure of *B. subtilis* GPATase (Smith et al., 1994) by truncation of nonidentical side chains to alanine and deletion of different-length loops and flexible peptides. Six orientations of the 222-symmetric probe were consistent with the self-rotation function, and were each refined by Patterson correlation (Brünger, 1990), with 112 individual secondary structural elements refined in the last cycle. Correlation coefficients were greater than 0.3 in all cases, although random orientations usually produce correlations less than 0.09 (Brünger, 1991). However, orientations with the molecular R axis along the crystallographic *b* axis produced the highest correlations. The approximate position of the tetramer within the unit cell was deduced by consideration of lattice packing and pseudo centering of the diffraction data. Care was taken to avoid a solution that was precisely C-centered.

The position and orientation of the molecular 222 symmetry were refined in the resulting electron density maps with the program LSQROT (AVGSYS programs by J.L. Smith & W.A. Hendrickson). Interpretable maps were produced using phase refinement and extension with programs from AVGSYS integrated into CCP4 (Bolin et al., 1993). In each cycle, the electron density map was modified by fourfold averaging, solvent flattening, and truncation of the lowest 10% of electron densities.  $|F_{calc}|$  values were substituted for unmeasured data in computation of unweighted electron density maps. Phase combination was not used.

Subsequent steps in the structure determination of GPATase consisted of several cycles of model building in O (Jones et al., 1991),

simulated annealing, and conventional refinement with X-PLOR (Brünger et al., 1990; Brünger, 1992) and TNT (Tronrud et al., 1987). When the better-diffracting C222<sub>1</sub> crystals and selenomethionyl protein became available, this model included 1,808 residues and had an *R*-factor of 24%. The model built and refined against the C222<sub>1</sub> data was used later to improve the P2<sub>1</sub>2<sub>1</sub> model by replacement of all but the PRTase active site with the 2.0-Å C222<sub>1</sub> model. During this process, the unit cell dimensions for the P2<sub>1</sub>2<sub>1</sub> crystal were adjusted by as much as 1% to the values given in Table 1, based on comparison of  $C_\alpha$  positions to the more accurate 2.0-Å model. This adjustment also resulted in lower RMSD values for superpositions of monomers in the P2<sub>1</sub>2<sub>1</sub> model. A significant improvement in the quality of electron density was produced, including interpretable density for most of the poorly ordered residues. Conventional refinement was performed in X-PLOR, employing noncrystallographic symmetry restraints between subunits containing AMP and between subunits without AMP. Restraints were divided into two structural domain cores and four smaller fragments. Final statistics for this model are given in Table 2. The model is deposited in the Protein Data Bank under code 1ecj.

#### Structure determination of the C222<sub>1</sub> crystal form

The highly similar dimensions of the two crystal forms suggested that the C222<sub>1</sub> lattice represents exact centering of the pseudo C-centered P2<sub>1</sub>2<sub>1</sub> crystal form. Space group P2<sub>1</sub>2<sub>1</sub> is one of the subgroups of space group C222<sub>1</sub>. One dimer of the P2<sub>1</sub>2<sub>1</sub> model in its crystallographic coordinate system was translated to align common symmetry operators with respect to the different origin convention of the standard C222<sub>1</sub> setting. The presumed relationship of the two crystal forms was confirmed by model refinement as multiple rigid bodies in X-PLOR, which produced an *R*-factor of 40.5% for reflections in the range 10.0–3.0 Å. Se positions for the SeMet protein, which generally corresponded to positions in the model, were readily located in a ( $|F_{SeMet}| - |F_{native}|$ ) difference map using phases from the rigid-body refined model. MLPHARE (Otwinowski, 1991) was used to refine the Se model and calculate SIR phase probabilities. Of 22 SeMet residues per dimer, 20 fully and 1 partially occupied Se sites were located, producing phases

**Table 2.** Refinement and model statistics

	AMP P2 <sub>1</sub> 2 <sub>1</sub>	No ligand C222 <sub>1</sub>
Range of data (Å)	30–2.5	30–2.0
No. reflections	54,315	65,453
No. atoms	15,688	8,859
No. waters	178	986
R-factor <sup>a</sup> (%)	18.1	17.5
R-free (%)	24.8	23.0
Average isotropic B-factor <sup>b</sup>	64.2	28.9
RMSD bonded B-factors	4.78	0.98
RMSDs from target values		
Bond lengths (Å)	0.008	0.011
Bond angles (°)	1.90	1.73
Torsion angles (°)	23.3	22.9
Noncrystallographic symmetry		
RMSD of C <sub>α</sub> positions (Å)	0.53	0.70

<sup>a</sup> $R = \sum |F_{obs} - F_{calc}| + \sum |F_{obs}|$ .

<sup>b</sup>Sums are weighted by atomic occupancies.

for data to 2.3 Å with a mean figure of merit of 0.54 for centric reflections, and 0.30 for all reflections.

Phases from the initial C222<sub>1</sub> model and SeMet SIR were combined to produce the starting phase set for refinement by twofold averaging and solvent flattening using software adapted from AVG-SYS and CCP4. A 2.8-Å electron density map was produced, which revealed additional electron density for approximately 100 residues in the dimer, and was used to construct a 94% complete model (950 residues). This model was subjected to simulated annealing refinement in X-PLOR, followed by several rounds of model building with O and conventional refinement in X-PLOR. Noncrystallographic symmetry restraints were not employed. Structure parameters for PIPES buffer molecules were derived from 12 small molecule structures in the Cambridge Structural Database (Allen & Kennard, 1993) using the LEARN function in X-PLOR. The final model for two subunits of the GPATase tetramer contains 992 of 1,008 amino acid residues and 982 water molecules. Statistics for this model are found in Table 2. The model is available in the Protein Data Bank under code 1ecf.

### Acknowledgments

Work was supported by NIH grants DK42303 to J.L.S. and GM24658 to H.Z.

### References

- Allen FH, Kennard O. 1993. 3D search and research using the Cambridge Structural Database. *Chemical Design Automation News* 8:31–37.
- Amann E, Ochs B, Abel KJ. 1988. Tightly regulated tac promoter vectors useful for the expression of unfused and fused proteins in *Escherichia coli*. *Gene* 69:301–315.
- Bolin JT, Smith JL, Muchmore SW. 1993. Considerations in phase refinement and extension: Experiments with a rapid and automatic procedure. *Abstracts of the American Crystallographic Association* 21:51.
- Brannigan JA, Dodson G, Duggleby HJ, Moody PCE, Smith JL, Tomchick DR, Murzin AG. 1995. A protein catalytic framework with an N-terminal nucleophile is capable of self-activation. *Nature* 378:416–419.
- Brünger AT. 1990. Extension of molecular replacement: A new search strategy based on Patterson correlation refinement. *Acta Crystallogr A* 46:46–57.
- Brünger AT. 1991. Solution of a Fab (26–10)/digoxin complex by generalized molecular replacement. *Acta Crystallogr A* 47:195–204.
- Brünger AT. 1992. *X-PLOR, version 3.1. A system for X-ray crystallography and NMR*. New Haven, Connecticut/London: Yale University Press.
- Brünger AT, Kruckowski A, Erickson JW. 1990. Slow-cooling protocols for crystallographic refinement by simulated annealing. *Acta Crystallogr A* 46:585–593.
- CCP4. 1994. Collaborative Computational Project, Number 4. The CCP4 suite: Programs for protein crystallography. *Acta Crystallogr D* 50:760–763. [SERC Daresbury Laboratory, Bailey S, contact person.]
- Chen S, Tomchick DR, Wolle D, Hu P, Smith JL, Switzer RL, Zalkin H. 1997. Mechanism of the synergistic endproduct regulation of *Bacillus subtilis* glutamine phosphoribosylpyrophosphate amidotransferase by nucleotides. *Biochemistry* 36:10718–10726.
- Eads JC, Scapin G, Xu Y, Grubmeyer C, Sacchettini JC. 1994. The crystal structure of human hypoxanthine-guanine phosphoribosyltransferase with bound GMP. *Cell* 78:325–334.
- Hendrickson WA, Horton JR, Lemaster DM. 1990. Selenomethionyl proteins produced for analysis by multiwavelength anomalous diffraction (MAD): A vehicle for direct determination of three-dimensional structure. *EMBO J* 9:1665–1672.
- Henrikson A, Aghajari N, Jensen KF, Gajhede M. 1996. A flexible loop at the dimer interface is a part of the active site of the adjacent monomer of *Escherichia coli* orotate phosphoribosyltransferase. *Biochemistry* 35:3803–3809.
- Higashii T. 1989. The processing of diffraction data taken on a screenless Weissenberg camera for macromolecular crystallography. *J Appl Crystallogr* 22:9–18.
- Isupov MN, Obmolova G, Butterworth S, Badet-Denisot MA, Badet B, Polikarpov I, Littlechild JA, Teplyakov A. 1996. Substrate binding is required for assembly of the active conformation of the catalytic site in Ntn amidotransferases: Evidence from the 1.8 Å crystal structure of the glutaminase domain of glucosamine 6-phosphate synthase. *Structure* 4:801–810.
- Jones TA, Zou JY, Cowan SW, Kjeldgaard M. 1991. Improved methods for building protein models in electron density maps and the location of errors in these models. *Acta Crystallogr A* 47:110–119.
- Kabsch W. 1988. Evaluation of single-crystal X-ray diffraction data from a position-sensitive detector. *J Appl Crystallogr* 21:916–924.
- Kim JH, Krahn JM, Tomchick DR, Smith JL, Zalkin H. 1996. Structure and function of the glutamine phosphoribosylpyrophosphate amidotransferase glutamine site and communication with the phosphoribosylpyrophosphate site. *J Biol Chem* 271:15549–15557.
- Kyte J. 1995. *Structure in protein chemistry*. New York/London: Garland Publishing, Inc. pp 64–69.
- McClard RW, Fischer AC, Mauldin SK, Jones ME. 1984. 5-Phosphorylribose 1- $\alpha$ -methylenebisphosphonate: Properties of a substrate analog of 5-phosphorylribose 1- $\alpha$ -diphosphate. *Bioorganic Chem* 12:339–348.
- Messenger LJ, Zalkin H. 1979. Glutamine phosphoribosylpyrophosphate amidotransferase from *Escherichia coli*: Purification and properties. *J Biol Chem* 254:3382–3392.
- Musick WDL. 1981. Structural features of the phosphoribosyltransferases and their relationship to the human deficiency disorders of purine and pyrimidine metabolism. *CRC Crit Rev Biochem* 11:1–34.
- Otwinowski Z. 1991. Maximum likelihood refinement of heavy atom parameters. In: Wolf W, Evans PR, Leslie AGW, eds. *Isomorphous replacement and anomalous scattering*. Daresbury, England: Science & Engineering Research Council. pp 80–86.
- Otwinowski Z. 1993. Oscillation data reduction program. In: Sawyer L, Isaacs N, Bailey S, eds. *Data collection and processing*. Daresbury, England: Science & Engineering Research Council. pp 56–62.
- Otwinowski Z, Minor W. 1997. Processing of X-ray diffraction data collected in oscillation mode. *Methods Enzymol* 276:307–326.
- Rossmann MG, Blow DM. 1962. The detection of sub-units within the crystallographic asymmetric unit. *Acta Crystallogr* 15:24–31.
- Rudolph J, Stubbe J. 1995. Investigation of the mechanism of phosphoribosylamine transfer from glutamine phosphoribosylpyrophosphate amidotransferase to glycaminide ribonucleotide synthetase. *Biochemistry* 34:2241–2250.
- Sakabe N. 1991. X-ray diffraction data collection system for modern protein crystallography with a Weissenberg camera and an imaging plate using synchrotron radiation. *Nucl Inst Meth Phys Res A* 303:448–463.
- Scapin G, Grubmeyer C, Sacchettini JC. 1994. Crystal structure of orotate phosphoribosyltransferase. *Biochemistry* 33:1287–1294.
- Scapin G, Ozkurt DH, Grubmeyer C, Sacchettini JC. 1995. The crystal structure of the orotate phosphoribosyltransferase complexed with orotate and  $\alpha$ -D-5-phosphoribosyl-1-pyrophosphate. *Biochemistry* 34:10744–10754.
- Schumacher MA, Carter D, Roos DS, Ullman B, Brennan RG. 1996. Crystal structures of *Toxoplasma gondii* HGXPRTase reveal the catalytic role of a long flexible loop. *Nature Struct Biol* 3:881–887.
- Smith JL. 1995. Structures of glutamine amidotransferases from the purine biosynthetic pathway. *Biochem Soc Trans* 23:894–898.

- Smith JL, Zaluzec EJ, Wery JP, Niu L, Switzer RL, Zalkin H, Satow Y. 1994. Structure of the allosteric regulatory enzyme of purine biosynthesis. *Science* 264:1427–1433.
- Somoza JR, Chin MS, Focia PJ, Wang CC, Fletterick RJ. 1996. Crystal structure of the hypoxanthine-guanine-xanthine phosphoribosyltransferase from the protozoan parasite *Tritrichomonas foetus*. *Biochemistry* 35:7032–7040.
- Stoker PW, O'Leary MH, Boehlein SK, Schuster SM, Richards NGJ. 1996. Probing the mechanism of nitrogen transfer in *Escherichia coli* asparagine synthetase by using heavy atom isotope effects. *Biochemistry* 35:3024–3030.
- Switzer RL. 1989. Non-redox roles for iron-sulfur clusters in enzymes. *BioFactors* 2:77–86.
- Tomchick DR, Smith JL, Wolle D, Zalkin H. 1994. Structure of *B. subtilis* glutamine PRPP amidotransferase at 2.3 Å and nucleotide binding studies. *Abstracts of the ACA, Series 2, vol 22*, p 49.
- Tong L, Rossmann MG. 1990. The locked rotation function. *Acta Crystallogr A* 46:783–792.
- Tronrud DE, Ten Eyck LF, Matthews BW. 1987. An efficient general-purpose least-squares refinement program for macromolecular structures. *Acta Crystallogr A* 43:489–501.
- Vos S, de Jersey J, Martin JL. 1997. Crystal structure of *Escherichia coli* xanthine phosphoribosyltransferase. *Biochemistry* 36:4125–4134.
- Wong JY, Bernlohr DA, Turnbough CL Jr, Switzer RL. 1981. Purification and properties of glutamine phosphoribosylpyrophosphate amidotransferase from *Bacillus subtilis*. *Biochemistry* 20:5669–5674.
- Wyngaarden JB. 1972. Glutamine phosphoribosylpyrophosphate amidotransferase. *Curr Topics Cell Regulation* 5:135–176.
- Zalkin H. 1993. The amidotransferases. *Adv Enzymol Relat Areas Mol Biol* 66:203–309.
- Zalkin H, Smith JL. 1998. Enzymes utilizing glutamine as an amide donor. *Adv Enzymol Relat Areas Mol Biol* 72. Forthcoming.
- Zhou G, Charbonneau H, Colman RF, Zalkin H. 1993. Identification of sites for feedback regulation of glutamine 5-phosphoribosylpyrophosphate amidotransferase by nucleotides and relationship to residues important for catalysis. *J Biol Chem* 268:10471–10481.
- Zhou G, Smith JL, Zalkin H. 1994. Binding of purine nucleotides to two regulatory sites results in synergistic feedback inhibition of glutamine 5-phosphoribosylpyrophosphate amidotransferase. *J Biol Chem* 269:6784–6789.